INSIGHTS INTO THE ELECTROLYTE CHANGES DURING THE ELECTRO-DEOXIDATION OF NIOBIUM OXIDE CATHODE

Amr M. Abdelkader

Faculty of Science and Technology, Bournemouth University, Talbot Campus, Fern Barrow, Poole, BH12 5BB, UK

Abstract

In the last two decades, tremendous work has been investigating the electro-reduction of metal oxide cathodes in what is known as the FFC-Cambridge process. This paper explores the electrolyte changes that occur during the electro-deoxidation of metal oxides. The investigation takes niobium oxide as a case study and subjects a Nb_2O_5 cathode to a constant potential difference of 2.5V, between the cathode and carbon anode during the in-*situ* recording of the cyclic voltammetry of the electrolyte on a glassy carbon electrode. The deoxidation of the cathode supplies oxygen ions that increase the oxygen content of the electrolyte, even in the very early stage of the process. We could detect many non-Faradic processes and increase the electrolyte electronic and ionic conductivity a few hours after starting the electro-deoxidation due to the reduction of CaO. It was also possible to detect partial dissolution of the cathode in the electrolyte and back deposition of Nb on the current collector. The dissolved niobium ions can combine with the oxide ion in the melt to form a negatively charged complex which can be discharged on the anode to form a thick ceramic layer. The electrolyte changes were also investigated using electrochemical impedance spectroscopy.

1 INTRODUCTION

The FFC-Cambridge process is a relatively new method to prepare metals and alloy powder starting from their oxides.[1] It conventionally employs a molten chloride salt, with a pure metal-oxide or a mixture of metal-oxides (MO) forming the cathode and graphite being employed as an anode. Upon applying a voltage lower than the decomposition voltage of the calcium chloride salt (3.2V), the metal oxide is reduced to form metal (M) and oxygen ions (O^{2-}) through reaction (1) without significant deposition of calcium. The oxygen ions diffuse through the molten bath to the positively charged electrode. Conventionally-used carbon anode reacts with these oxygen ions to form carbon oxide gases (CO, CO_2) at the anode (reactions 2, and 3) [2-4].

$$MO + 2e^- \rightarrow M + O^{2-} \tag{1}$$

$$C + 2O^{2-} = CO_2 + 4e^- \tag{2}$$

$$2C + 2O^{2-} = 2CO + 4e^- \tag{3}$$
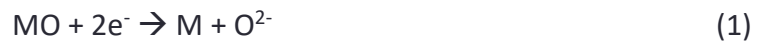
A significant amount of work has since been focused on the electrolytic production of numerous metals, alloys, and carbides directly from their metal-oxides (such as: Al_2O_3, Cr_2O_3, SiO_2, CuO, Fe_2O_3, Nb_2O_3, Ta_2O_5, SiO_2, UO_2, V_2O_3, WO_3, HfO_2 and ZrO_2)[3, 5-17]. The majority of the research was devoted to the cathode reactions, with very few works discussing the anode or the electrolyte processes. Despite intensive research during the last two decades, some issues still exist in fully understanding the electrolyte processes and the electrolyte /electrode interactions. [18, 19]These include; partial or full dissolution of some oxides in the molten salt, the nature of the ions (or complexes) in the electrolyte, and the current loss due to the melt's electronic conductivity. Furthermore, understanding the electrolyte processes may lead to better control and increase the current efficiency by minimising the parasitic electrolyte reactions. Therefore, the present work aims to study the changes in the electrolyte's properties during the electro-deoxidation, using niobium oxide as an example. A series of cyclic voltammograms of the electrolyte was recorded on a glassy carbon electrode after different electro-deoxidation intervals, which were then correlated to the processes at the cathode. Niobium oxide was chosen as a cathode material due to the numerous investigations carried out to study the cathodic

reactions, which ensures that the cathodic part of the process is well known, and allows direct comparison with the results obtained during this research whilst focusing on the electrolyte reactions [9, 20, 21].

2 EXPERIMENTS:

Niobium pentoxide (99.99 %, Aldrich, 20851-5) was used to form the metal-oxide cathode in this investigation. The mean particle size for the as-received powder was measured using a particle sizing machine (Malvern, Mastersizer 2000) to be 6.03μm. The oxide powders were uniaxially pressed, at 20MPa, using a 25mm die, into 4g pellets. The pellets were sintered at 1373K for 2.5 hours, which resulted in a total porosity of 34%. General grade graphite rod (10 mm diameter, Tokai, HK-0) and glassy carbon (4mm diameter, HTW GmbH, Sigadur G) was used as the anode and reference electrode, respectively.

Calcium chloride is the most common electrolyte used in the FFC-Cambridge Process[3]. Therefore, calcium chloride was selected as the electrolyte for this study and was prepared by the thermal drying of calcium chloride di-hydrate (Fisher, C/1500/65) in a vacuum, as described in previous work [22, 23]. To distinguish between the oxide ions produced through the electro-deoxidation process and that already exist as impurities in the electrolyte, ultra-oxide-free melts were used as an electrolyte in the current work. These oxide-free salts were produced by an extra vacuum drying step at 523 K of the dehydrated $CaCl_2$ in *situ* prior to heating the salt to the melting temperature. Typically the dehydrated $CaCl_2$ was placed in the electrolysis crucible, and the reactor vessel was evacuated using an Edwards RV3 pump. The temperature increased by 2 K/min till 523 K and dwelled for 3 hours under vacuum before the system was filled with Ar gas. The reactor was then heated to 1173 K at 2 K/min and held at this temperature until the run ended. Pre-electrolysis was applied for 2 hours using a voltage of 2V applied across two graphite rods to remove electroactive impurities and residual water from the salt. These two rods were slowly raised to the cooler top part of the reactor.

The molten salt reactor used in the electrochemical experiments was assembled using an INCONEL® tube housed in a Vecstar® vertical furnace. The molten salt reactor

used in the electrochemical experiments was assembled using an INCONEL® tube housed in a Vecstar® vertical furnace. The niobium oxide precursors were drilled to accept a 2mm diameter nickel wire cathode collector (99.95%, Advent, Ni5355). The carbon anode was attached to the connection lead by making a 2mm wide and a 0.5mm deep cut around the top and wrapping the nickel wire once around this groove. This method was also used to make an electrical connection to the graphite pseudo-reference electrode. This type of reference electrode has been used by several authors [24, 25]. It was employed in this work because it avoids other materials that may contaminate the melt, an important precaution in experiments using low oxide concentrations.

The constant voltage experiments were conducted using a PSS-210-GW INSTEK programmable power supply. This device was equipped with Instek PSU software to record the variation of current versus time as well as the potential. The constant voltage experiments were interrupted after different times to record the cyclic voltammograms of the electrolyte. The CVs were achieved using a glassy carbon working electrode at a scan rate of 50 mV/S using the Solartron® RSI 1287 electrochemical interface.

A similar setup was used for the electrochemical impedance spectroscopy (EIS). To focus the investigation into the electrolyte changes, we replaced the Ni-Nb$_2$O$_3$ electrode with Mo wire and the graphite counter electrode with a glassy carbon rod. After each interval of the constant voltage experiments, the niobium oxide cathode and the carbon anode were lifted to 2 cm above the salts. Then, the new electrodes were slowly lowered into the electrolyte. All the EIS were conducted with the frequency range of 10 kHz to 0.01 Hz and perturbation amplitude of 10 mV.

The phase compositions of the samples were characterised through X-ray diffraction analysis (Phillips, PW1050), with the scan range set from 10º to 80º. The microstructure and chemical composition of the samples were investigated by JSM-5800LV, JEOL scanning electron microscopy (SEM) equipped with an energy-dispersive X-ray analyser (EDX) at an accelerating voltage of 15kV. Non-conductive samples were sputter-coated with gold using Emitech K550 sputter coater.
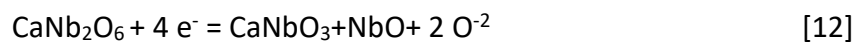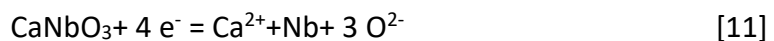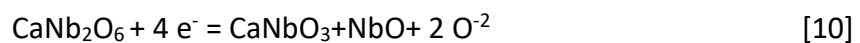
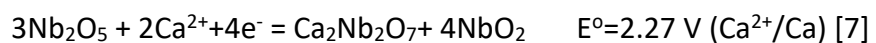## 3   RESULTS AND DISCUSSION:

3.1   AN OVERVIEW OF THE CATHODIC REACTIONS:

As the initial oxide content of $CaCl_2$ melt is a function of the drying procedure, it was necessary to prepare an oxide-free electrolyte by having an extra drying step in the reactor vessel and just before applying the voltage. Therefore, the electro-deoxidation of Nb_2O_5 was carried out at a constant voltage of 2.5 V. The Nb_2O_5 cathode pellet was about 4g, and a graphite rod was used as an anode. Figure 1 shows the recorded time-current curve during the course of electro-deoxidation. The time-current curve showed five distinguished features: (1) a rapid increase in the first few minutes due to the fast metallisation of the high resistance oxide at the surface layer; (2) an intermediate shoulder (feature A-B in figure 1) indicating the slow reduction progressing in the interior part of the pellet; (3) a fast decline between features B and C; (4) a pseudo shoulder between C and D; and (5) a gradual decrease tending to the background current starting from feature E.

A series of partially reduced samples were collected from a sequence of constant voltage experiments conducted for different periods. Figure 2 summarises the XRD analysis of the resulting samples, and Figure 3 shows the SEM image of the final Nb product. From the XRD pattern, one can conclude the following mechanism for the electro-deoxidation of Nb_2O_5: The process started by calcium ion and oxygen ion insertion into the oxide at the cathode, forming calcium niobate of the same oxidation state ($CaNb_2O_6$ and $Ca_2Nb_2O_7$ through equations 4 and 5). It should be noted that there is no reduction at this stage.

$$Ca^{2+} + O^{2-} + Nb_2O_5 = CaNb_2O_6 \qquad [4]$$

$$2Ca^{2+} + 2O^{2-} + Nb_2O_5 = Ca_2Nb_2O_7 \qquad [5]$$

The reduction during this stage is negligible; therefore, the current showed a shoulder between 5 to 60 minutes (feature A-B in figure 1). Once some of the oxygen ions in the Nb(V) compounds were removed and the non-stoichiometric phase $Ca_3Nb_2O_{8-x}$ formed, the reduction proceeded faster, associated with a fast decline in the current (feature B-C). The reduction rate slowed as soon as $Ca_3Nb_2O_{8-x}$ converted to compounds of the fourth oxidation state ($CaNbO_3$ and NbO_2). Nb(IV) is then reduced to Nb(II) through reaction (6) and then to Nb(O) through reaction (7), with the current gradually decreasing to its background level (features C-E). It is also worth mentioning that there is not enough evidence to exclude the direct formation of Nb(II) from Nb(IV) through reaction (8) or the direct reduction of $CaNbO_3$ to metallic niobium through reaction (11). In addition, $CaNb_2O_4$, in which niobium ions exist as Nb(III), was detected as traces in some experiments associated with $CaNbO_3$, NbO_2 and Nb. Although the intermediate phase $CaNb_2O_4$ was not consistently detected, the transformation from $CaNbO_3$ to Nb logically passed through $CaNb_2O_4$ at high temperature, but the Nb(III) compound dissociated upon cooling to Nb and Nb(IV)[26]. A detailed study of the reduction mechanism can be found in our pervious work.
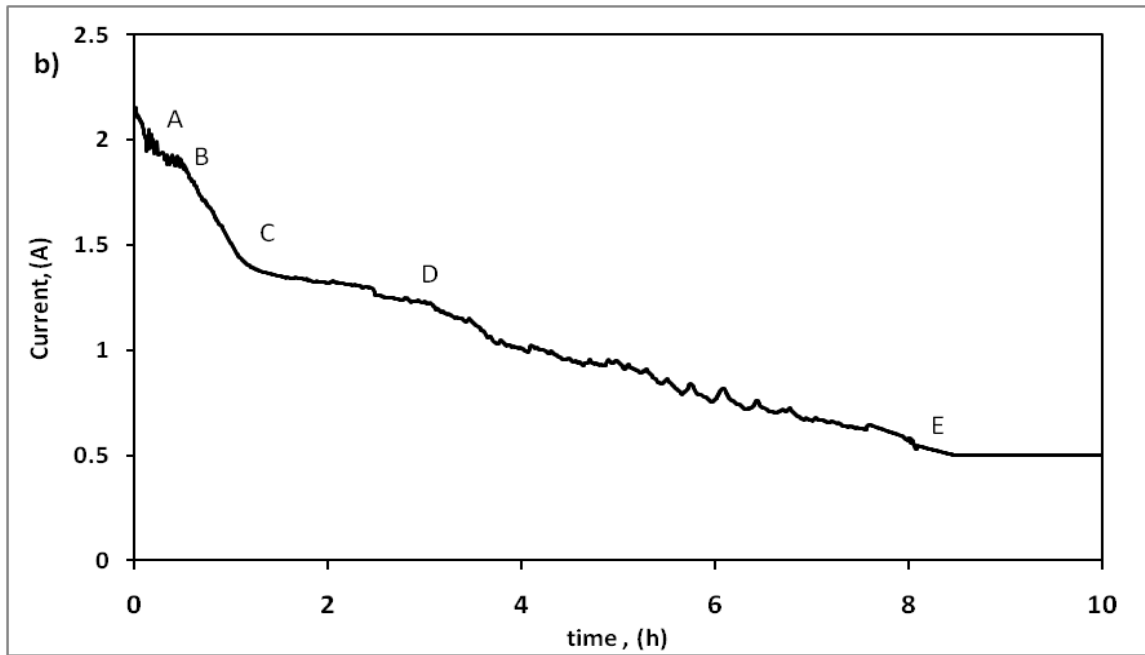
$$2Nb_2O_5 + Ca^{2+} + 2e^- = CaNb_2O_6 + 2NbO_2 \qquad E^o=2.27 \text{ V } (Ca^{2+}/Ca) \text{ [6]}$$

$$3Nb_2O_5 + 2Ca^{2+} + 4e^- = Ca_2Nb_2O_7 + 4NbO_2 \qquad E^o=2.27 \text{ V } (Ca^{2+}/Ca) \text{ [7]}$$

$$CaNbO_3 + 4e^- = Ca^{2+} + NbO + 2O^{2-} \qquad [8]$$

$$NbO + 2e^- = Nb+ + O^{2-} \qquad E^o=1.03 \text{ V } (Ca^{2+}/Ca) \text{ [9]}$$

$$CaNb_2O_6 + 4e^- = CaNbO_3 + NbO + 2O^{-2} \qquad [10]$$

$$CaNbO_3 + 4e^- = Ca^{2+} + Nb + 3O^{2-} \qquad [11]$$

$$CaNb_2O_6 + 4e^- = CaNbO_3 + NbO + 2O^{-2} \qquad [12]$$

FIGURE 1: current-time curve for Nb_2O_5 pellet reduced at constant voltage of 2.5 V in molten $CaCl_2$- 1 mol.% CaO melt.
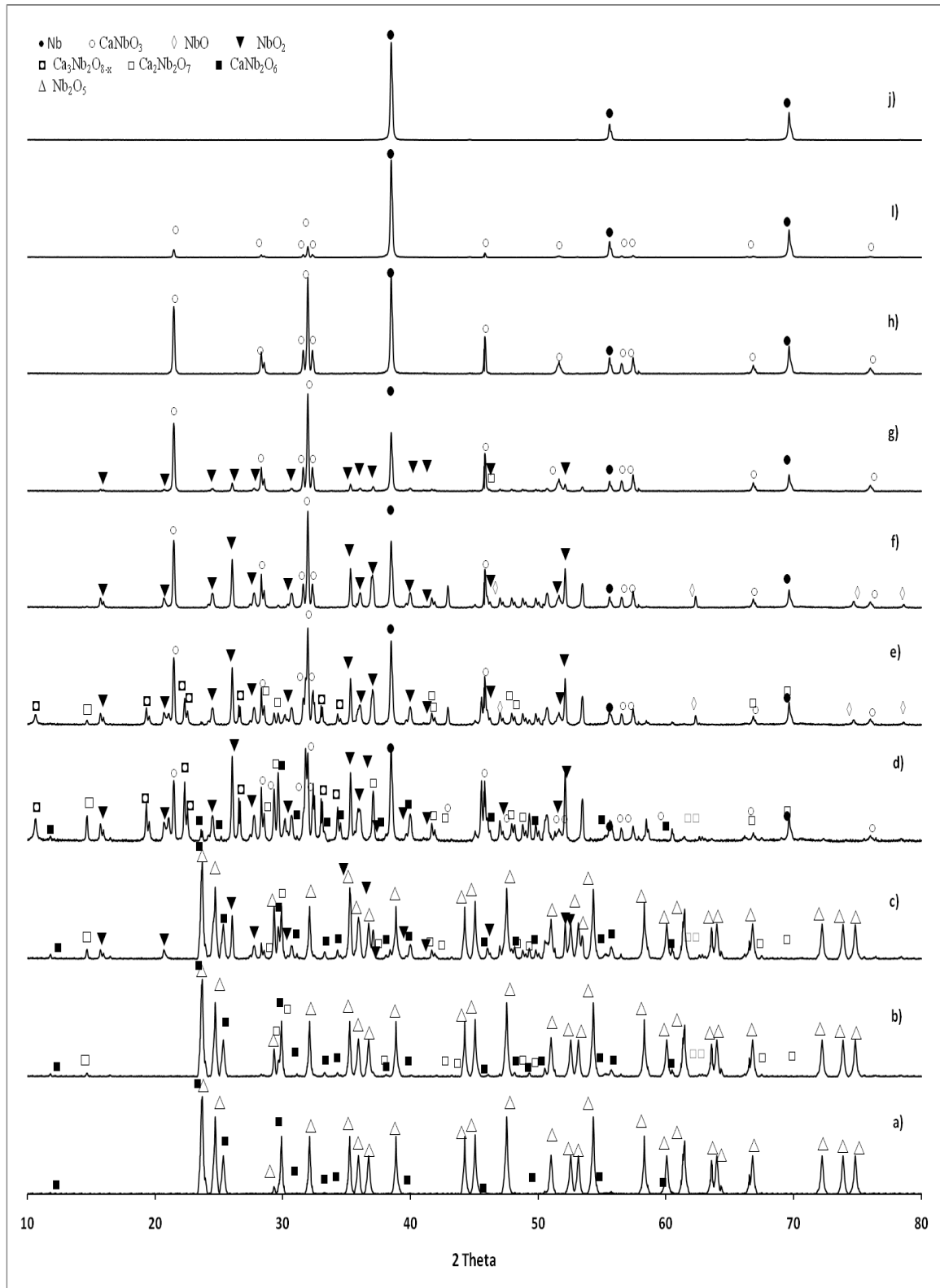
FIGURE 2: XRD traces of the Nb_2O_5 pellet electro-deoxidised in molten $CaCl_2$ at 2.5 V recorded after (a) 10 minutes, (b) 30 minutes, (c) 60 minutes, (d) 90 minutes, (e) 120 minutes, (f) 2.5 hours, (g) 3 hours, (h) 4 hours, (I) 5 hours, and (j) 6 hours of polarisation.
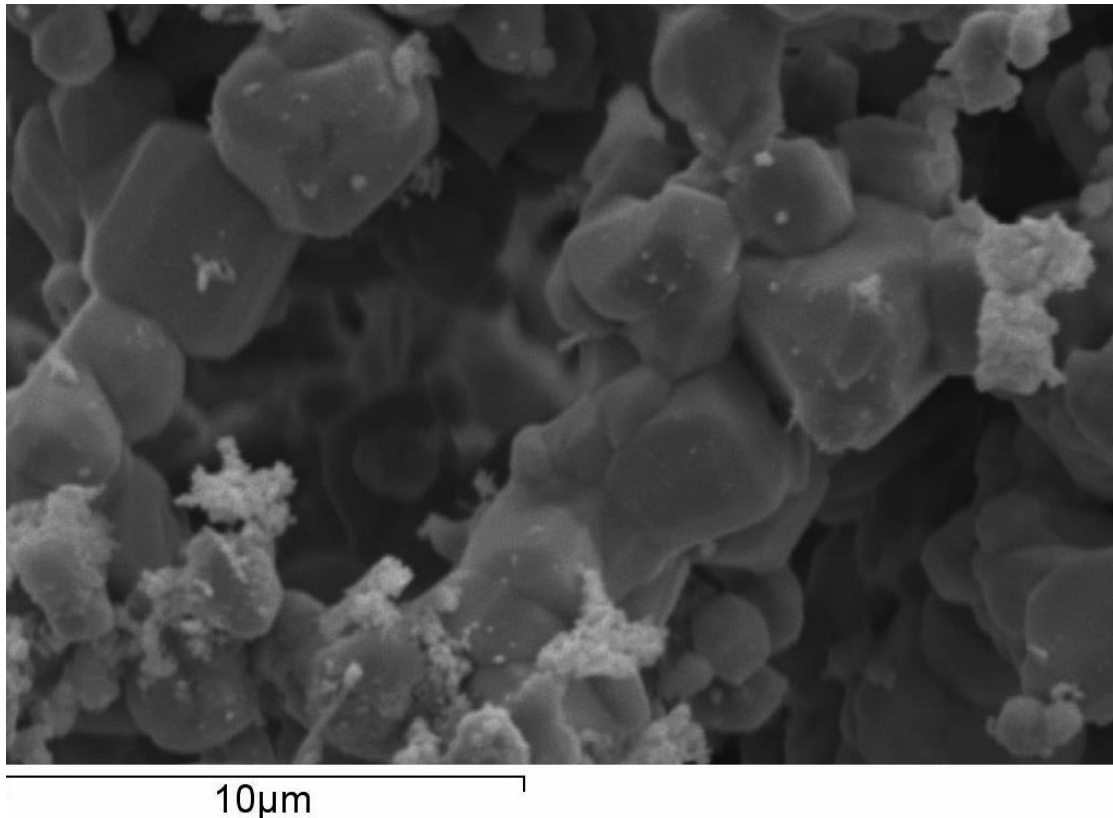
FIGURE 3: SEM image of the produced niobium showing the cubic grains that tends to agglomerate together in larger clusters.

3.2 CYCLIC VOLTAMMETRY STUDY FOR THE ELECTROLYTE PROCESSES:

The electrochemical window of the oxide-free melt was measured on a glassy carbon working electrode, as illustrated in figure 4. The voltammogram shows two couples of peaks: one in the cathodic and one in the anodic scan. The cathodic one at −1.3 V versus graphite is believed to be the deposition of calcium metal, while the peak observed in the anodic scan is believed to correspond to the formation of Cl_2 gas. The reverse background current showed the same value as the forward one when extensive calcium deposition was avoided, indicating that almost zero non-faradic currents passed in the electrolyte. Between calcium deposition and chlorine formation, the CV is featureless, meaning no electrochemical processes are taking place on the working electrode due to the absence of electroactive species in the electrolyte. It should be noted here that the electrochemical window of the oxide-free electrolyte is only ~2.6 V. The theoretical decomposition voltage of $CaCl_2$ is around
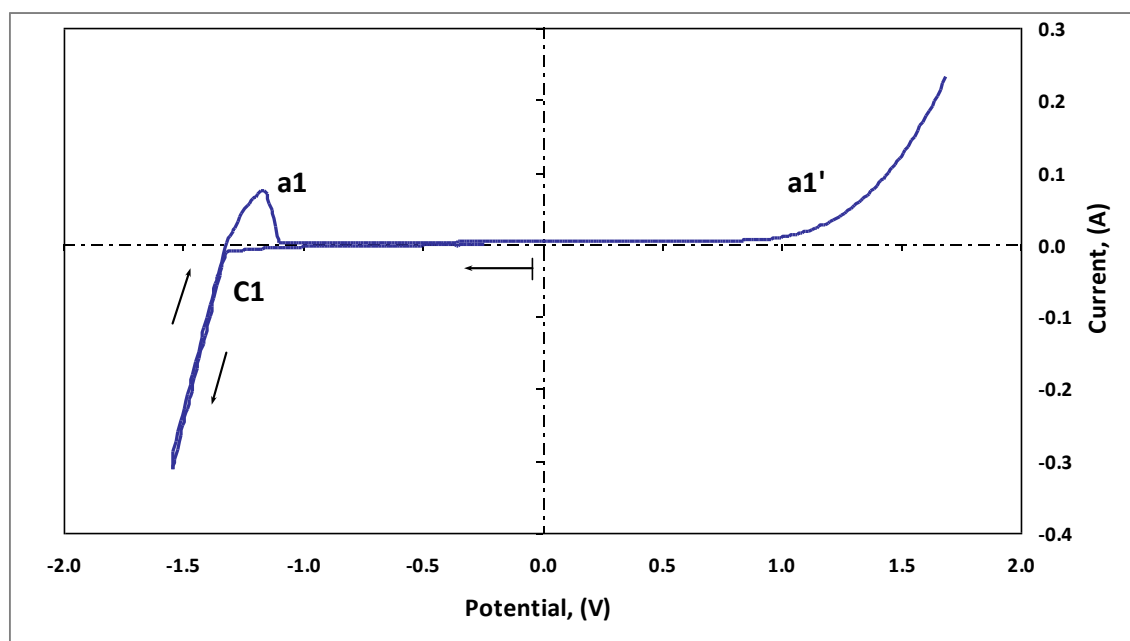
FIGURE 4: The electrochemical window of the oxide-free CaCl₂ at 1173 K measured at a 0.1 V/S scan rate.

A pellet of 4g of Nb_2O_5 was then immersed in the salt, and a 2.5 V constant voltage was applied between the pellet and carbon anode for 30 minutes. After this short electro-deoxidation run, the cyclic voltammogram of the melt (Figure 5) showed an extra oxidation peak at about 0.7 V versus the graphite pseudo reference (+2 V versus Ca/Ca^{+2}). This peak is at the same position as the carbon oxide generation peak previously observed when CaO was added to the melt [27-29]. Indeed, the oxide ions observed in the present case must be generated by reducing the Nb_2O_5 pellet at the cathode, as there were no other sources of oxides in the cell. Detection of this peak suggests oxide ions accumulation in the electrolyte due to a slower discharge of ions on the anode rather than producing them from the cathode. The peak position and current had not changed when the cyclic voltammogram was recorded for the salt after 1 hour of electro-deoxidation. For both voltammograms, i.e. after 30 minutes and 1 hour, the value of current in the forward and reverse scan was almost the same, suggesting no electronic conductivity of the salt up to this stage.
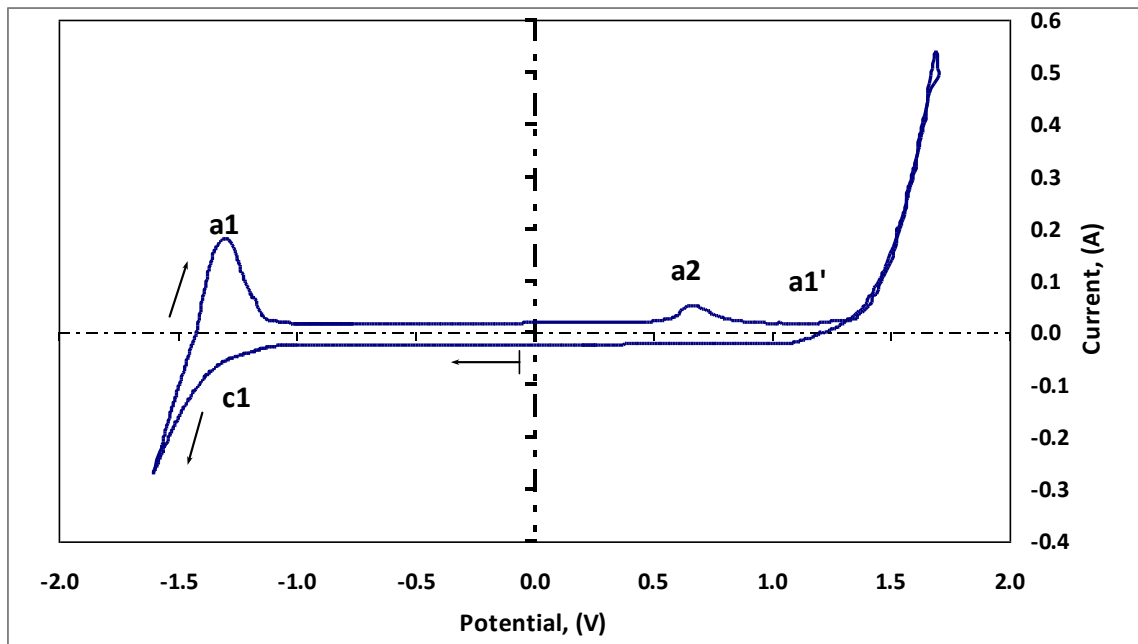
FIGURE 5: Cyclic voltammogram of CaCl$_2$ melt after 30 minutes of electro-deoxidising a pellet of Nb$_2$O$_5$ at 3 V.

The literature has reported that under constant voltage conditions, calcium metal may start depositing from the CaO dissolved in 1mol.% CaO-CaCl$_2$ melt.[30, 31] In the present case, the activity of the CaO in the melt is expected to be lower. However, incorporating CaO (in the form of diatomic or polyatomic ions) from the reduction of the calcium niobate phase on the cathode raised the calcium ions' activity and made calcium deposition possible. Figure 6 proves more calcium deposition from the melt, as the I$_p$ value of the calcium dissolution peak increased with the electro-deoxidation time. Moreover, the voltammogram recorded for the melt after 3 hours of electro-deoxidation (figure 7) showed about 0.2 A gap between the forward and reverse current, suggesting double layer capacitance (ECDL). This ECDL could be attrbuited to increasing the ionic conductivity of the melt and also the cathode specific surface area when the oxide ions migrate toward the electrolyte.
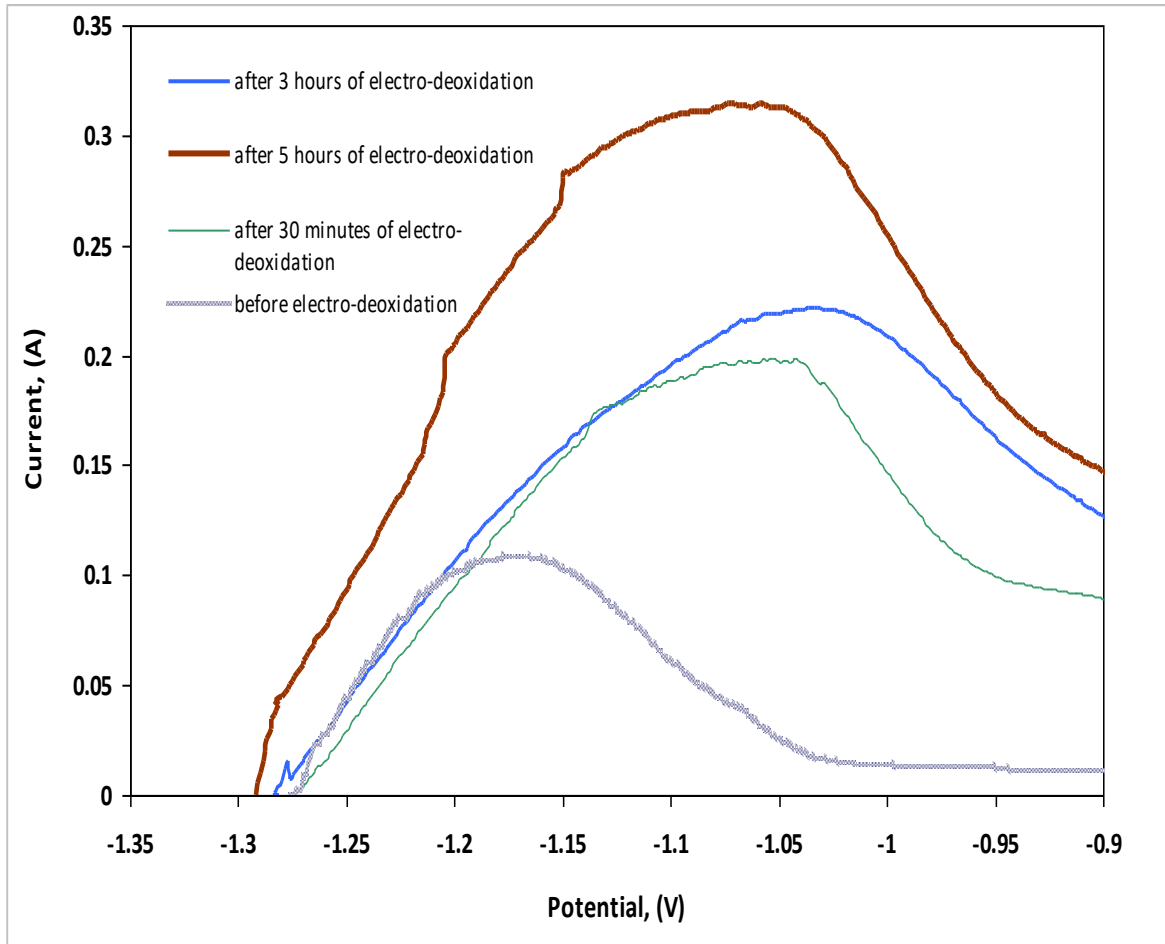
FIGURE 6: Calcium dissolution peak (peak a1) recorded for the CaCl₂ melt after different times of electro-deoxidising a pellet of Nb₂O₅.
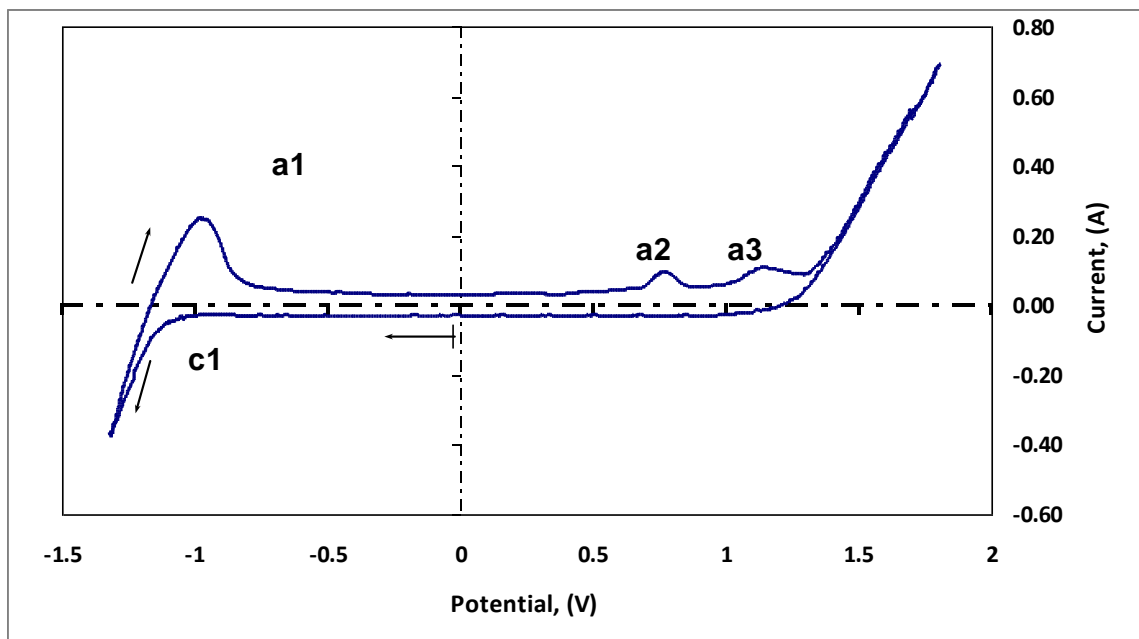

FIGURE 7: Cyclic voltammogram of CaCl₂ melt after 3 hours of electro-deoxidising a pellet of Nb₂O₅ at 3 V.

The voltammogram recorded after 3 hours showed an additional irreversible oxidation peak (a3) at 1.2 V versus a graphite pseudo reference (Figure 7). Mohamedi et al.[32] detected two oxidation peaks in the system CaO-$CaCl_2$ and referred them to the reaction of carbon with oxide ions in two steps: firstly, the discharge of oxide anions (O^{-2}) and formation of adsorbed C_xO species; and second, the reaction of C_xO with more discharged oxide anions forming gaseous CO_2 and small amounts of carbon. The absence of the second oxidation peak in the voltammogram recorded after 1 and 2 hours of the electro-deoxidation suggests the second peak (a3) is a function of the oxide ion content in the electrolyte. The formation of CO_2 was confirmed by running a controlled experiment at a contest potential equal to a3 (1.2 V vs carbon). The exhaust gasses were passed through a flask filled with limewater. The limewater turned into a cloudy solution and white precipitates of calcium carbonate could be observed at the bottom of the flask, confirming peak a3 is for CO_2 gas formation.

After 5 hours of electro-deoxidation, the cyclic voltammogram detected another reversible reduction peak (c2) at about 0.3 V versus Ca/Ca^{+2}, as illustrated in figure 8. Dissolution of the cathode materials during the reduction of NbO to niobium was previously reported. Therefore, peak (c2) is more likely due to the dissolved Nb(II) ions in the electrolyte being deposited on the cathode before being re-dissolved in the corresponding oxidation wave(a0). Therefore, it is worth here to focus on peaks (c2) and (a0) and investigate them further to gain information on the kinetics and mechanisms of the relevant electrode processes:
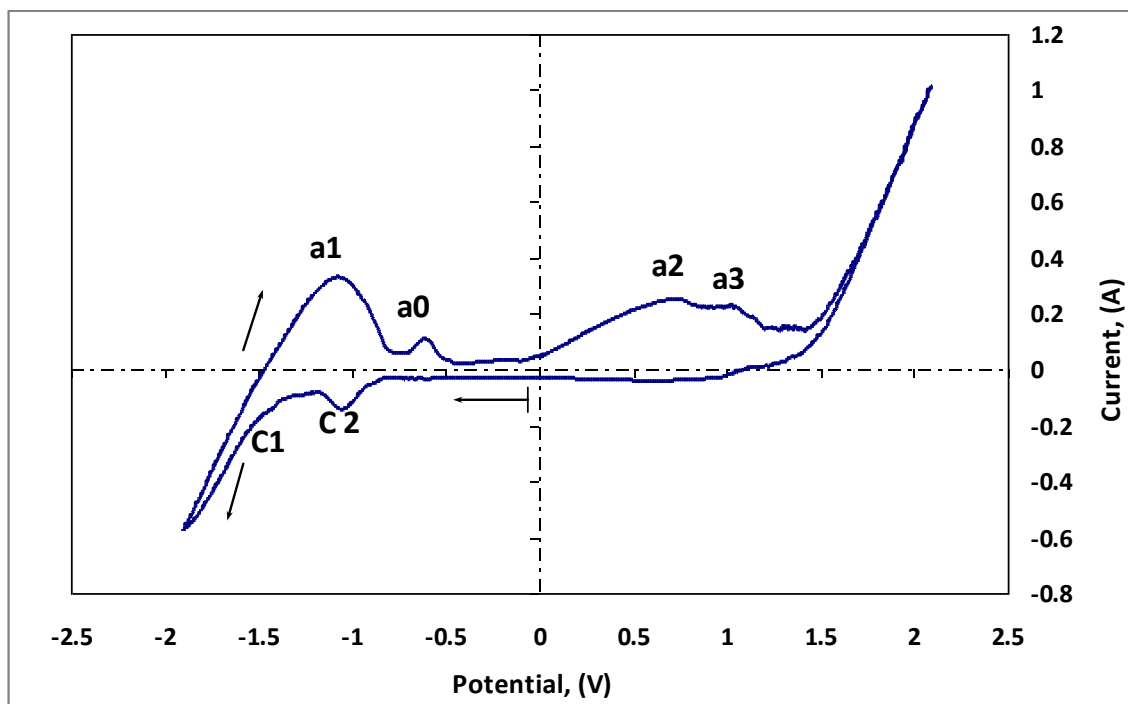
FIGURE 8: Cyclic voltammogram of CaCl$_2$ melt after 5 hours of electro-deoxidising a pellet of Nb$_2$O$_5$ at 3 V.

A series of cyclic voltammograms were carried out at different potential sweep rates (ν) ranging from 50 mV to 2 V. Values of the cathodic peak current density I$_P$ was plotted against $\nu^{1/2}$ (figure 9). The resulting plot shows a linear relation of I$_P$ versus $\nu^{1/2}$, which is a typical feature for a diffusion-controlled charge-transfer process with no chemical complications [32]. The cathodic peak potential remained almost constant when the potential sweep rate increased. For a reversible electrode reaction involving the deposition of an insoluble substance, the value $|E_p- E_{p/2}|$ is equal to 0.77RT/nF. The measured $|E_p- E_{p/2}|$ value was found to be 39mV at a scan rate lower than 0.05 V/S. Giving n=2 electrons; 0.77RT/nF gives a value of 38mV, further proving that peak (c2) is due to the reduction of Nb^{+2}. The deviation of $|E_p- E_{p/2}|$ from the theoretical value at a high scan rate might be referred to as the ohmic drop interferences because of the high current flowing through the electrode.
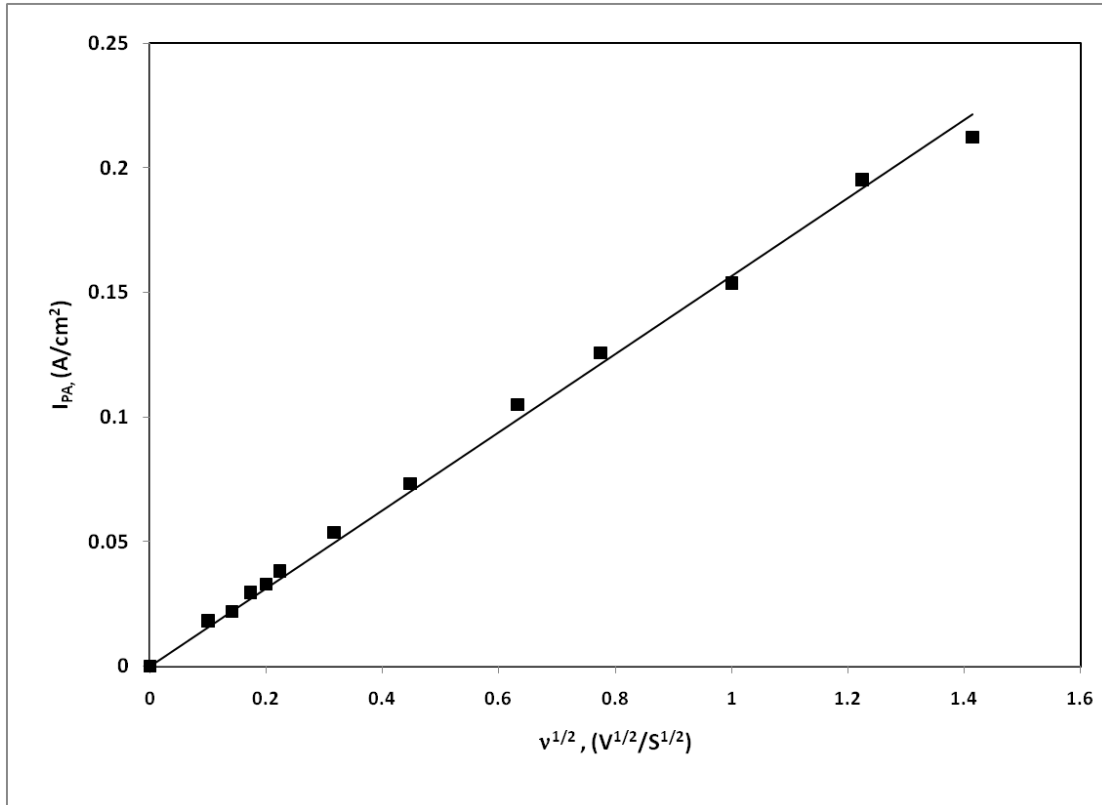
Figure 9: The dependencies of peak C2 currents of the redox process on the polarisation rate.

After 8 hours of electro-deoxidation, the niobium ions vanished from the salt and deposited on the metallic parts of the cathode assemblage. Therefore, it was not surprising that the Nb^{+2}/Nb redox couple peaks disappeared from the voltammogram recorded after 8 hours of electro-deoxidation (Figure 10). On the other hand, a cathodic peak was observed at 0.15 V versus Ca/Ca^{+2}, with no corresponding peak in the reverse scan. Based on the EDX analysing of the deposit at the stainless steel cathode after electro-deoxidising Nb_2O_5 for 8 hours and the detection of carbonaceous materials, the peak (c3) might be related to the reduction of carbon-containing complexes. Suppose this complex is carbon-oxygen (including CO_3^{-2}) or carbon-calcium. In that case, no new peaks will be observed in the reverse scan as the oxidation peaks will be in the same position as calcium dissolution and/or carbon oxidation peaks. Hence, the assumption that peak (c3) is for carbon-containing complex finds some support from the absence of new peaks in the oxidation scanning. The reduction of carbon-containing ions may explain the carbide phases previously reported to contaminate the cathode product after electro-deoxidation[9].
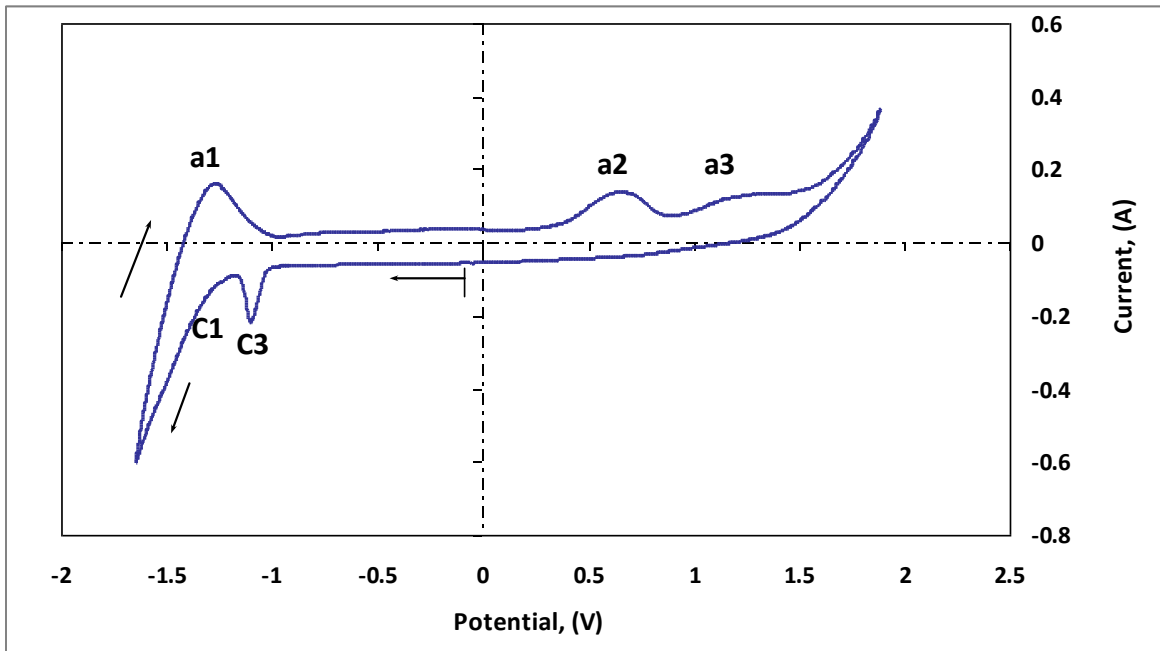
Upon increasing the oxide activity in the initial salt, i.e. using the system CaO-CaCl$_2$, the recorded voltammogram in the first 5 hours was in general similar to that when oxide-free electrolyte was used. However, there are a few differences: (I) The carbon oxidation peaks (a2 and a3) shifted slightly to more positive values, and the current density of the peaks I$_{pa2}$ and I$_{pa3}$ increased in response to increasing the oxy-anion species in the electrolyte. (II) The difference between the background current in the forward and the reverse scan was higher (ranging from 100 to a few hundred mA), reflecting high electronic conductivity in the melt. Figure (11) shows the voltammogram recorded for the CaO-CaCl$_2$ electrolyte after different periods of electro-deoxidation. (III) The difference between the measured potential for the deposition of calcium (peak c1) and the oxidation of Cl$^-$ to Cl$_2$ (peak a1') is lower (ranging between 2.1 V to 2.6 V) when CaO was added to the melt. These values are also lower than the calculated value of CaCl$_2$ or even CaO dissociation and might be attributed to the calcium metal that dissolved in the electrolyte from the electro-deoxidation process.
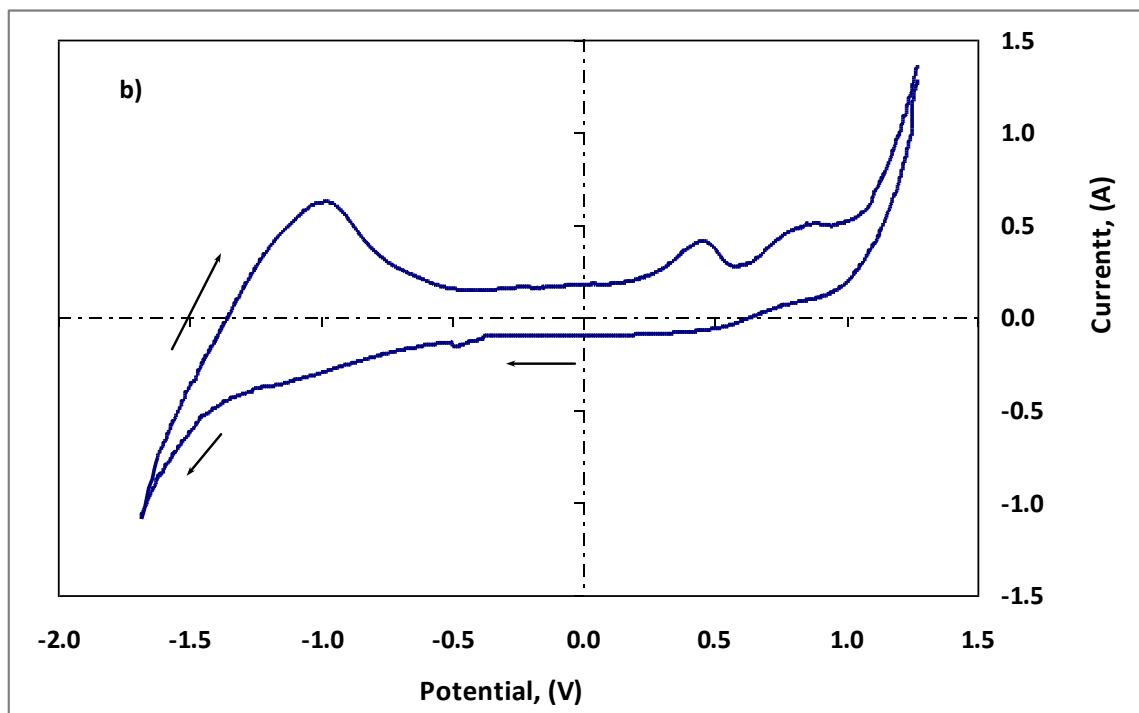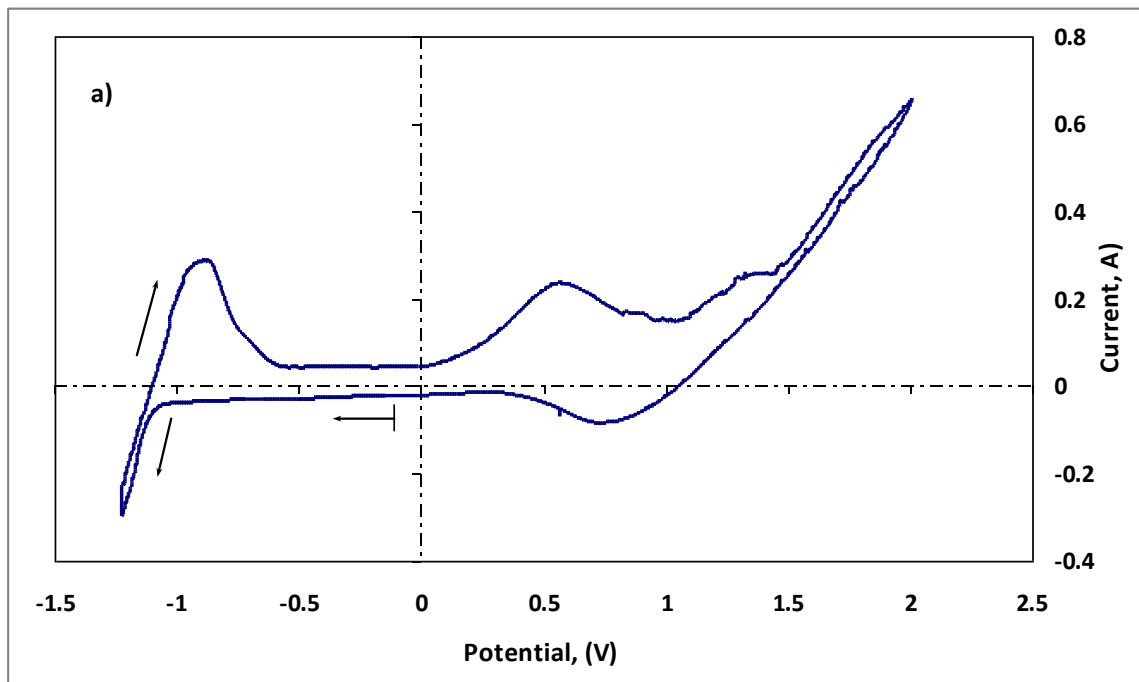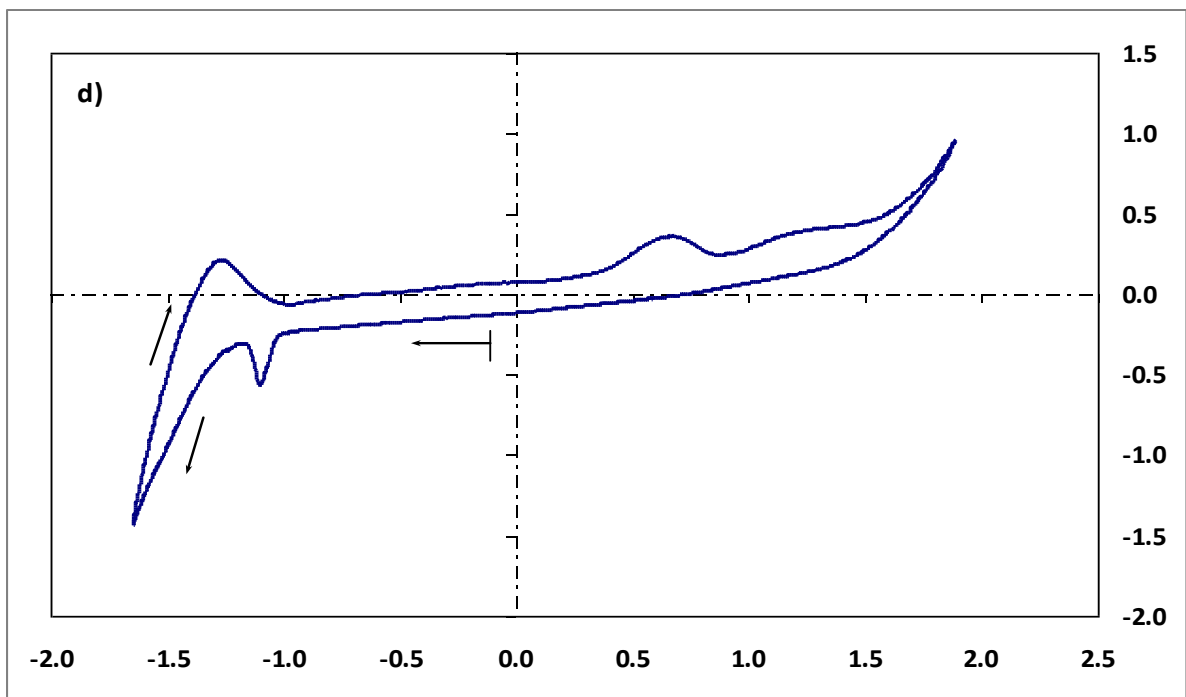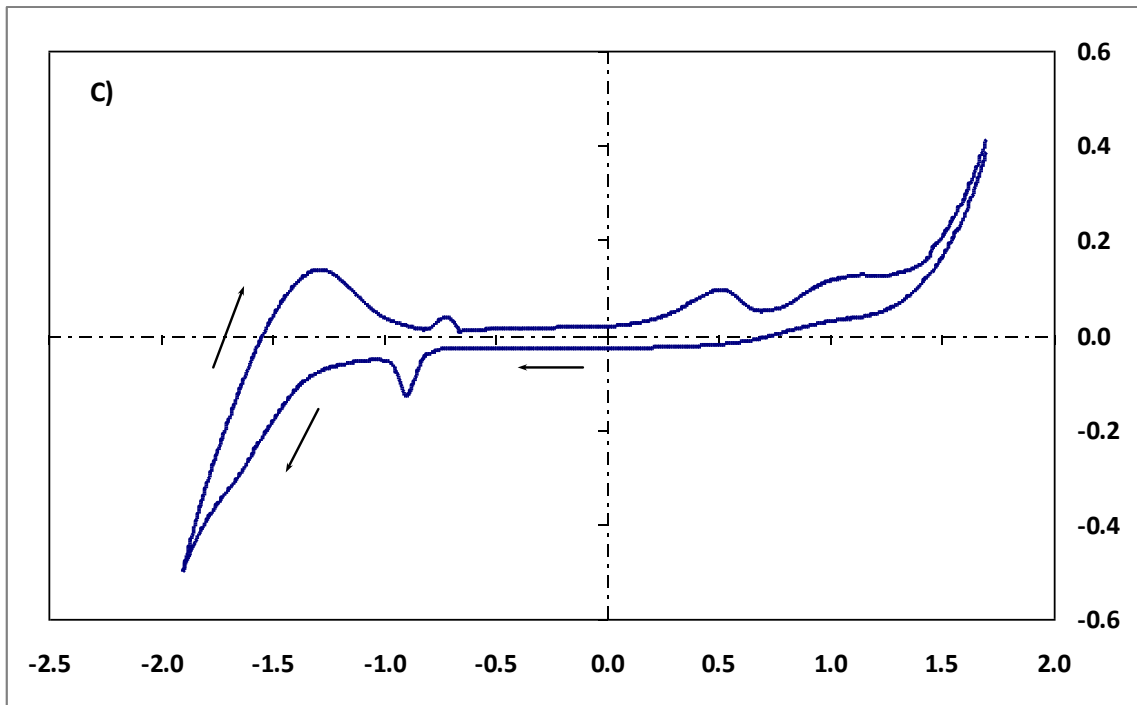
FIGURE 11: Cyclic voltammograms of CaO-CaCl$_2$ melt after electro-deoxidation of Nb$_2$O$_5$ pellet at 3 V for (a) 1 hours, (b) 2 hours, (c) 3 hours, and (d) 5 hours.

The reduction is generally quicker when CaO is present in the salt. An example is the Nb(II) reduction peak (peak C2), which was observed after a shorter time when CaO was added to the electrolyte. The voltammogram recorded for the 1 mol. % CaO-CaCl$_2$ system, after electro-deoxidising a pellet of Nb$_2$O$_5$ for 3 hours, detected the Nb^{+2}/Nb redox couple peaks almost in the same position as was in the case of the oxide-free electrolyte. However, the reduction peak current increased, and the oxidation peak decreased when CaO was added to the melt, giving insight that the reduction of Nb(II) ions is not fully reversible in high oxide content electrolytes. Moreover, the value |Ep- E$_{p/2}$| was found to be 10 times larger than the theoretical value for a reversible process involving a two-electron exchange (0.39 V at 1173 K). As this insoluble substance was not observed in the oxide-free electrolyte, it is more likely to be one of the insoluble niobium oxides or complexes with calcium. This assumption finds evidenced by the presence of white powder on the electrode after the end of the cyclic voltammetry experiments figure S5.

Linking the cyclic voltammetry results with the real electro-deoxidation experiments might give more insights into the nature and mechanism that leads to the formation of this white insoluble oxide from the reduction of the dissolved Nb(II). The graphite anode after electro-deoxidation of Nb$_2$O$_5$ for 8 hours in 1mol. % CaO-CaCl$_2$ has a grey layer of Nb$_2$O$_5$ and NbO$_2$. Figure S6 shows the deposited layer on the graphite anode. The grey colour of the deposit is probably due to some carbonaceous materials on the oxide layer. Detection of such a layer on the anode means Nb(II) ions in the electrolyte could form some negatively charged complexes in the high oxide ions activity electrolyte. This agrees with Schwandt et al. , who also detected CaTiO$_3$ on the anode when TiO$_2$ was electro-deoxidised in the CaO-CaCl$_2$ molten bath.

3.3 ELECTROCHEMICAL IMPEDANCE SPECTROSCOPY STUDY OF THE ELECTROLYTE.

More insights about the electrolyte changes during the course of the reduction process can be obtained from the electrochemical impedance. The Nyquist plot before and after different periods of electro-deoxidation is illustrated in Figure S1 (Supporting information). The impedance spectrum of the oxide-free electrolyte before the process is irregular, with a high impedance of about 10^4 Ω. The electrolyte, after 30 min of electro-deoxidation, showed different features. There is a clear loop at high

frequency, suggesting an increase in the ionic conductivity and initiating a double-layer capacitance, in line with the CV results. After 1 hour of the process, a well-formed loop at high frequency and a straight line at low frequency can be observed. This typical feature of a diffusion-controlled process suggests the ions concentration is high enough to crowd the processes at the working Mo electrode. The semicircle at the high frequency gets smaller for the electrolyte after 3 and 5 hours of the electro-deoxidation. The small semicircle means the mobility of the ions is improving, and the processes at the Mo/electrolyte interface are not limited by charge transfer. The first part of the Nyquist plot represents the electrolyte electrical resistance (R_e). Thus, the diffusion-controlled process on a Mo electrode can be represented by the circuit in figure S2 (supporting information).

The emergence of Warburg resistance at the low frequency after less than an hour of the electrolysing may indicate that a porous deposit partially covers the Mo working electrode surface. The decrease in the line slope with the electro-reduction time suggests this porous deposit is thicker and more hindrance to the charge transfer. The EDX analysis could detect Nb on the Mo surface, further proving the partial dissolution of the cathode materials. It should be noted that the Re value significantly decreases with the progress of the electro-deoxidation, which could be attributed to the change of the electrolyte compositions, as discussed with the CV results.

4   CONCLUSION:

The electrolyte processes that take place during the electro-deoxidation of metal oxide have been studied in situ using cyclic voltammetry and niobium oxide as the cathode materials. The cyclic voltammetry detected an increase in the non-faradic current during the process, despite the applied potential being lower than the decomposition potential of the electrolyte. The oxygen content of the oxide-free electrolyte was found to depend on the rate of the cathodic reactions that produce oxide ions. The CV also detected the reduction of carbon-containing ions on the cathode, which may explain the detection of carbide phases previously reported on the cathode product. Partial loss of cathode materials was detected and referred to

as the dissolution of the NbO intermediate phase. It was found that the dissolved NbO ions tend to form a negatively charged complex when the electrolyte has high oxides ions activity.

5 REFERENCES

1. Choi, E.-Y. and S.M. Jeong, *Electrochemical processing of spent nuclear fuels: An overview of oxide reduction in pyroprocessing technology.* Progress in Natural Science: Materials International, 2015. **25**(6): p. 572-582.
2. Chen, G.Z., D.J. Fray, and T.W. Farthing, *Direct electrochemical reduction of titanium dioxide to titanium in molten calcium chloride.* Nature, 2000. **407**(6802): p. 361-364.
3. Abdelkader, A.M., et al., *DC voltammetry of electro-deoxidation of solid oxides.* Chemical Reviews, 2013. **113**(5): p. 2863-2886.
4. Abdelkader, A., et al., *DC voltammetry of electro-deoxidation of solid oxides.* Chemical reviews, 2013. **113**(5): p. 2863-2886.
5. Wang, D., X. Jin, and G.Z. Chen, *Solid state reactions: an electrochemical approach in molten salts.* Annual Reports on the Progress of Chemistry - Section C, 2008. **104**: p. 45.
6. Barnett, R.P. and D.J. Fray, *Reaction of tantalum oxide with calcium chloride-calcium oxide melts.* Journal of Materials Science, 2013. **48**(6): p. 2581-2589.
7. Abdelkader, A.M. and D.J. Fray, *Electrochemical synthesis of hafnium carbide powder in molten chloride bath and its densification.* Journal of the European Ceramic Society, 2012. **32**(16): p. 4481-4487.
8. Abdelkader, A.M. and D.J. Fray, *Synthesis of self-passivated, and carbide-stabilised zirconium nanopowder.* Journal of Nanoparticle Research, 2013. **15**(12): p. 1-8.
9. Abdelkader, A.M. and D.J. Fray, *Direct electrochemical preparation of Nb-10Hf-1Ti alloy.* Electrochimica Acta, 2010. **55**(8): p. 2924-2931.
10. Abdelkader, A.M. and D.J. Fray, *Electro-deoxidation of hafnium dioxide and niobia-doped hafnium dioxide in molten calcium chloride.* Electrochimica Acta, 2012. **64**: p. 10-16.
11. Bhagat, R., et al., *In situ synchrotron diffraction of the electrochemical reduction pathway of TiO2.* Acta Materialia, 2010. **58**(15): p. 5057-5062.
12. Bhagat, R., et al., *The production of Ti-Mo alloys from mixed oxide precursors via the FFC cambridge process.* Journal of the Electrochemical Society, 2008. **155**(6): p. E63-E69.
13. Cox, A. and D. Fray, *Mechanistic investigation into the electrolytic formation of iron from iron(III) oxide in molten sodium hydroxide.* Journal of Applied Electrochemistry, 2008. **38**(10): p. 1401-1407.
14. Peng, J.J., et al., *Phase-Tunable Fabrication of Consolidated (alpha plus beta)-TiZr Alloys for Biomedical Applications through Molten Salt Electrolysis of Solid Oxides.* Chemistry of Materials, 2009. **21**(21): p. 5187-5195.
15. Abdelkader, A.M., *Molten salts electrochemical synthesis of Cr2AlC.* Journal of the European Ceramic Society, 2016. **36**(1): p. 33-42.
16. Dong, Y., et al., *Low-Temperature Molten-Salt Production of Silicon Nanowires by the Electrochemical Reduction of CaSiO3.* Angewandte Chemie, 2017. **129**(46): p. 14645-14649.
17. Qu, J., et al., *Revealing the mechanism of solid-state electrochemical conversion reactions in strong alkaline solutions.* Chemical Engineering Journal, 2021. **426**: p. 131307.
18. Zhang, C., et al., *Electroanalytical Measurements of Oxide Ions in Molten CaCl2 on W electrode.* Journal of The Electrochemical Society, 2021. **168**(9): p. 097502.
19. Kong, Y., et al., *Proving the Availability of Ni–Fe Anode for Electro-Reduction of Solid V2O3 in Molten Fluoride Salts.* Journal of The Electrochemical Society, 2021. **168**(11): p. 113505.
20. Xu, Q. and D.J. Fray, *Nb-Ta alloy powder by electrochemical reduction of Nb2O 5/Ta2O5 mixture in the CaCl2-NaCl melt*. 2011. p. 1131-1135.
21. Yan, X.Y. and D.J. Fray, *Electrochemical studies on reduction of solid Nb2O5 in molten CaCl2-NaCl eutectic II. Cathodic processes in electrodeoxidation of solid Nb2O5.* Journal of the Electrochemical Society, 2005. **152**(10): p. E308-E318.

22.   Barnett, R., K.T. Kilby, and D.J. Fray, *Reduction of Tantalum Pentoxide Using Graphite and Tin-Oxide-Based Anodes via the FFC-Cambridge Process.* Metallurgical and Materials Transactions B-Process Metallurgy and Materials Processing Science, 2009. **40**(2): p. 150-157.

23.   Abdelkader, A.M., et al., *Electrochemical synthesis and characterisation of a NdCo5 permanent magnet.* Journal of Materials Chemistry, 2010. **20**(29): p. 6039-6049.

24.   Schwandt, C., D.T.L. Alexander, and D.J. Fray, *The electro-deoxidation of porous titanium dioxide precursors in molten calcium chloride under cathodic potential control.* Electrochimica Acta, 2009. **54**(14): p. 3819-3829.

25.   Schwandt, C. and D.J. Fray, *The electrochemical reduction of chromium sesquioxide in molten calcium chloride under cathodic potential control.* Zeitschrift Fur Naturforschung Section a-a Journal of Physical Sciences, 2007. **62**(10-11): p. 655-670.

26.   Kumada, N. and N. Kinomiura, *Preparation and Crystal Structure of a New Reduced Calcium Niobium Oxide: CaNb2O4.* Journal of Solid State Chemistry, 1999. **147**(2): p. 671-675.

27.   Dukovic, J. and C.W. Tobias, *The Influence of Attached Bubbles on Potential Drop and Current Distribution at Gas-Evolving Electrodes.* Journal of the Electrochemical Society, 1987. **134**(2): p. 331-343.

28.   Vogt, H., *Contribution to the interpretation of the anode effect.* Electrochimica Acta, 1997. **42**(17): p. 2695-2705.

29.   Vogt, H., *Mechanisms of Mass-Transfer of Dissolved-Gas from a Gas-Evolving Electrode and Their Effect on Mass-Transfer Coefficient and Concentration Overpotential.* Journal of Applied Electrochemistry, 1989. **19**(5): p. 713-719.

30.   Abdelkader, A.M. and E. El-Kashif, *Calciothermic reduction of zirconium oxide in molten CaCl2.* ISIJ international, 2007. **47**(1): p. 25-31.

31.   Abdelkader, A. and A. Daher, *Preparation of hafnium powder by calciothermic reduction of HfO2 in molten chloride bath.* Journal of Alloys and Compounds, 2009. **469**(1-2): p. 571-575.

32.   Mohamedi, M., et al., *Anodic behavior of carbon electrodes in CaO-CaCl2 melts at 1123 K.* Journal of the Electrochemical Society, 1999. **146**(4): p. 1472-1477.